

Distributed acoustic sensing, transfer functions, and moment magnitude determination: Application to high-frequency downhole data

Boris Boullenger¹, Antony Butcher², Bob Paap¹, Vincent Vandeweijer¹, and Anna L. Stork³

ABSTRACT

Distributed acoustic sensing (DAS) enables sampling seismic wavefields along optical fibers at a spatial resolution of less than 1 m, over distances beyond several tens of kilometers. This makes DAS a powerful tool to record seismic events densely along 2D directions, whether horizontally along the earth's surface or vertically in boreholes. Compared with traditional seismic sensors measuring ground motion units, DAS provides uniaxial strain measurements along the fiber with often imperfectly known transfer functions between the measurements and true ground motion. This can generate uncertainties in the derivation of seismic source parameters, such as the magnitude, that require an absolute measurement of the ground motion and a known instrument response. In this study, we examine the DAS transfer function, mapping DAS data to reference velocity records obtained from multiple colocated accelerometers. Our investigation makes use of downhole recordings from the Frontier Observatory for Research in Geothermal Energy field site situated in Utah, USA. Overall, we find that the DAS response estimated at different depth positions follows a consistent trend and deviates significantly from a flat response only below 80 Hz. An average site-specific DAS system response is then used to convert microseismic event recordings into calibrated velocity records with improved amplitude accuracies. Subsequently, moment magnitudes M_W are derived from the P-wave records with results matching the independent accelerometerbased estimations with high fidelity for events with $M_W > -1.0$.

INTRODUCTION

Distributed acoustic sensing (DAS) refers to an ensemble of technologies that measure dynamic strain along optical fibers and that have been applied to a variety of geophysical applications. These include downhole seismic imaging and monitoring using a dedicated fiber (Mateeva et al. 2013, 2014; Daley et al. 2014, 2016; Karrenbach et al., 2019; Lellouch et al., 2019) and studies of earthquake and ambient-noise seismology (Hudson et al., 2021; Zhou et al., 2022).

One of the attractive properties of DAS arrays is that seismic wavefields can be sampled with spatial resolutions that are prohibitively expensive and often unfeasible using networks of traditional seismic sensors. The DAS arrays require significantly less effort to deploy, which is a big advantage in locations with difficult access, and increasingly there is a focus on exploiting existing fiber networks (Lindsey et al., 2017; Martin et al., 2017; Ajo-Franklin et al., 2019). For monitoring purposes in particular, downhole DAS is regarded as an efficient technology, for example, for the monitoring of induced seismicity in the context of hydraulic fracturing, geothermal production, or geologic storage of CO2.

A drawback of DAS data is that it typically suffers from lower signal-to-noise ratios (S/N) compared with those obtained from geophone sensors. This is partially due to the noise produced by the optical measurement process via the interrogator (Lindsey et al., 2020) but it is also due to the imperfect nature of the coupling of the fiber with its cable and/or of the cable with the surrounding

Manuscript received by the Editor 24 January 2024; revised manuscript received 27 September 2024; published ahead of production 24 January 2025; published online 26 March 2025.

TNO, Geological Survey of the Netherlands, Utrecht, The Netherlands. E-mail: boris.boullenger@tno.nl (corresponding author); bob.paap@tno.nl; vincent.vandeweijer@tno.nl.

University of Bristol, School of Earth Sciences, Bristol, UK. E-mail: antony.butcher@bristol.ac.uk.

³Silixa Ltd., Elstree, UK. E-mail: anna.stork@lunainc.com.

^{© 2025} The Authors. Published by the Society of Exploration Geophysicists. All article content, except where otherwise noted (including republished material), is licensed under a Creative Commons Attribution 4.0 International License (CC BY). See https://creativecommons.org/licenses/by/4.0/. Distribution or reproduction of this work in whole or in part commercially or noncommercially requires full attribution of the original publication, including its digital object identifier (DOI).

medium. The determination of these coupling effects remains challenging for DAS arrays, as these installations display a range of characteristics from site to site.

Another limitation of DAS is that the physical quantities that can be measured along the fiber are strain (dimensionless) or strain rate (in .s⁻¹) whereas some algorithms require ground motion quantities as direct input. For example, this is the case for methods to determine earthquake source parameters (Cole et al., 2018), such as the moment magnitude, which is often the preferred earthquake scale as it is directly related to fault dimensions, the amount of fault slip, and energy release (Kendall et al., 2019). In this context, Lior et al. (2023) propose a real-time conversion of strain rate to ground motion for the purpose of using DAS data in earthquake early warning systems. But the conversion does not take into account possible deviations of the DAS system response from a flat response, including uncertainties about the coupling quality of the fiber.

The preceding challenges can be addressed by estimating DAS transfer functions, which convert strain measurements into ground motion records. The transfer functions, including the conversion of physical units and coupling effects, can be combined into a single function referred to as the DAS system response (the DAS instrument response per se and the coupling effects together). This is the subject of a few pioneering studies, showing that a DAS system response can be quantified empirically across various frequency ranges through the analyses of DAS data colocated with measurements from reference seismic instrumentation (Jousset et al., 2018; Lindsey et al., 2020; Paitz et al., 2021). In these studies, the DAS system response estimation is preceded by a conversion of the original strain measurements into ground motion units. This conversion has been generally performed in studies especially focusing on the comparison of DAS and geophone data (Bóna et al., 2017; Wang et al., 2018; Zulic et al., 2022). The DAS system response is then quantified by extracting the frequency-dependent amplitude and phase responses using the DAS-derived and colocated geophone ground motion records.

Although many efforts have focused on determining the DAS system response for broadband tele-seismic earthquakes, there are no comprehensive demonstrations of applying such workflow to the higher frequency range of downhole DAS microseismic records, such as the derivation of calibrated ground motion records and moment magnitudes of the events. To this end, other studies have either developed scaling relationships between DAS amplitude and earth-

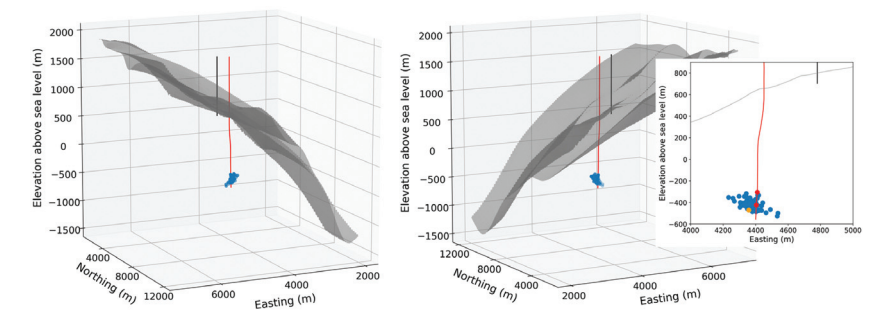


Figure 1. Geometry of the stimulation well (in red) and monitoring well (in black) at the FORGE site with local coordinates. The gray surface indicates the interface between the granitoid and the overlaying sediments. The locations of perforation shots 1 (lower shot) and 2 (upper shot) are indicated by the red dots in the right panel. The blue dots indicate the 110 microseismic-event locations. The selected event with $M_W = -0.68$ (27) April 2019, 20:20:57 UTC) is highlighted in orange.

quake magnitudes (Yin et al., 2023) or estimated moment magnitudes directly from low-frequency DAS strain records while accounting for polarization effects (Nayak et al., 2024). Distinctively, the moment magnitude estimation method we use is based on the prior conversion of DAS strain records to ground motion units, calibrated by correcting for the estimated DAS system response.

In this paper, we determine a DAS system response using a highfrequency downhole DAS data set from the Frontier Observatory for Research in Geothermal Energy (FORGE) geothermal site (Moore et al., 2019), for which several colocated reference measurements from accelerometers are available. The colocated data from two perforation shots originating in a nearby well are compared and used to estimate the DAS system response from a Silixa Carina system within the 20-200 Hz frequency range. In addition, we use the estimated DAS system response to retrieve calibrated velocity records from the DAS strain measurements. These calibrated records are used to measure M_W for previously detected microseismic events, and the DAS moment magnitude workflow results are compared with independently reported results obtained from the accelerometer data.

SITE AND FIELD DATA

The downhole field data set used in this study was acquired at the FORGE of the U.S. Department of Energy, located in Utah, USA. FORGE is a field laboratory site that was created to test and develop innovative technologies for enhanced geothermal systems. Various installations have been dedicated to the monitoring and study of induced seismicity, especially during campaigns of hydraulic stimulations that aimed at increasing the rock permeability within the geothermal reservoir. This includes a 1 km deep monitoring well in which an optical fiber is permanently cemented behind the casing. At the time of stimulations, the monitoring well is equipped with a string of 12 regularly spaced (30.5 m) 3C accelerometers (Versatile Seismic Imager, VSI, tool from Schlumberger). Although the fiber spans the entire depth range of the monitoring well, the point-sensor string merely covers the 650-970 m depth range.

Figure 1 shows the overall geometry of the site with the respective locations of the monitoring well and the well in which stimulations are performed. The stimulation well is approximately 2200 m deep and is perforated at two depth levels during the campaign. The perforation shots, approximately located at a horizontal distance of 370 m and at a depth of 1200 m with respect to the bottom of

> the monitoring well, provide high-frequency records from known locations that we use in this study to determine the DAS system response. Figure 1 also shows the locations of the 110 induced microseismic events detected from the DAS array by Lellouch et al. (2020), focusing on a 24 h window on 27-28 April 2019. Here, these catalogued events are used to test the reliability of determining moment magnitudes (M_W) from the DAS records after correcting for the DAS system response. The event catalogue provided by the contractor indicates that the M_W value range of the cloud is from $M_W = -1.68$ to $M_W = -0.5$. One of the strongest events ($M_W = -0.68$, on 27 April, 20:20:57 UTC), already selected for illustration in Lellouch et al. (2020), is used as an example for the DAS ground motion conversion workflow.

In the monitoring well, the optical fiber and its associated interrogator are elements of the Silixa Carina system, which produced continuous DAS data with a 10 m gauge length, a channel spacing of 1.02 m and a sampling frequency of 2000 Hz. Furthermore, the original measurements of optical-phase changes were directly converted into strain rate (measured in nm/m per second). The data from the string of accelerometers corresponds to ground acceleration measurements in m.s⁻², with a sampling frequency of 2000 Hz. The instrument response of the accelerometers is known and flat in the 2-200 Hz frequency range.

The DAS and accelerometer records are preprocessed similarly by applying linear detrending, mean removal, and a 10-400 Hz band-pass filter. However, the raw data from the DAS array suffers from relatively strong common mode noise caused by vibrations on the interrogator (Miller et al., 2018). Therefore, the DAS data processing first includes a filtering of the near-zero vertical wavenumbers (k_z) using a cosine taper in the frequency-wavenumber $(f-k_z)$ domain. The resulting strain rate and colocated vertical acceleration records for the perforation shots and the selected microseis-

mic event are shown in Figure 2. The two perforation shots contain the first incident P wave followed by weaker secondary P waves. S-wave energy can be found (from 0.15 s after the first Pwave arrival) but remains comparatively much weaker and so is not directly visible in the figure. However, the microseismic event, associated with a different source mechanism, contains much stronger S waves, visible from 0.15 s after the first P-wave arrivals. In all the three examples, the lower bound of the frequency range in which the recorded signals dominate the noise level is approximately 20 Hz. Consequently, our analysis of the DAS system response focuses on the 20-200 Hz, for which both the instrument response of the accelerometers is known and the seismic-event signals are prominent over noise. The accelerometer at position 9 is not included in the analysis because it was observed to be faulty.

In spite of the preprocessing, some DAS data remain locally contaminated with noisy channels. Other positions are affected by transient noise. To obtain a better assessment of the space and time distribution of this noise, we compute for each seismic event the amplitude spectrum averaged over three 2.5 s noise windows (time windows before and after the event) and over 30 adjacent channels centered at each position (Figure 2b, 2d, and 2f). The amplitudes for position 12 stand out significantly because the average includes few bottom channels affected by end-of-fiber effects. The results highlight overall depth positions consistently affected by stronger noise levels (positions 10, 11, 12 and, to a lesser extent, position 3). This also shows channels around position 4 are noisy during perforation shot 2. The spectrum amplitude values for the other positions (1, 2, 5, 6, 7, and 8) are all contained within a narrow minimum range, which indicates favorable S/N and a first evidence of a relatively consistent coupling conditions of the fiber for those positions.

DAS SYSTEM RESPONSE METHODOLOGY

The workflow used to determine and apply the DAS transfer function is composed of three steps: the conversion of preprocessed DAS data from strain to particle velocity units, the estimation of the DAS system response, and its removal from DAS-based velocity records.

Conversion to velocity units

Here, we assume that the fiber is straight and positioned vertically in the casing. As a result, we define the strain measured by the fiber as $\mathbf{E}_{z}(z,t)$ in the time domain. This quantity is related to its associated vertical particle velocity and can be expressed via the apparent velocity c_7 (m/s) (Aki and Richards, 2002) as

$$V_z^{\text{DAS}}(z,t) = -c_z(z,t)E_z(z,t), \tag{1}$$

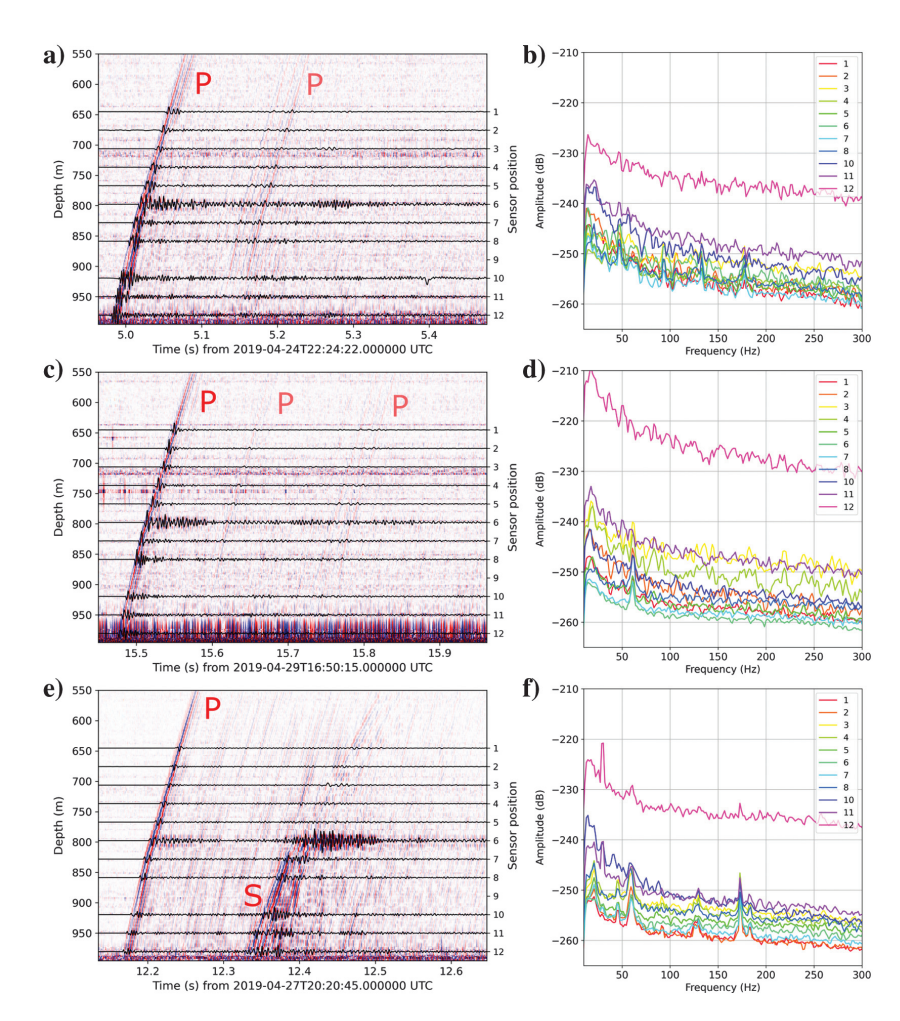


Figure 2. (a) Processed DAS strain rate records and colocated accelerometer data for perforation shot 1 (24 April 2019, 22:24:27 UTC). (b) Averaged amplitude power spectrum of DAS noise around each position: average over three 2.5 s noise windows and over 30 adjacent channels centered at the given position, (c and d) same as in (a and b) but for perforation shot 2 (29 April 2019, 16:50:30 UTC), and (e and f) same as in (a and b) but for the selected microseismic event (27 April 2019, 20:20:57 UTC). Prominent P- and S-wave arrivals are indicated in red in the left panels.

where $V_z^{\rm DAS}$ is the ground velocity that can be retrieved from the DAS strain measurements. Equation 1 shows that the ground velocity can be obtained by scaling the measured strain by c_z . As obtaining accurate apparent phase velocities is often challenging, several authors have proposed performing the scaling in the frequency-vertical-wavenumber (f-kz) domain (Daley et al., 2016; Lindsey et al., 2020). In the $f-k_z$ domain, equation 1 becomes

$$V_z^{\rm DAS}(k_z,\omega) = -\frac{\omega}{k_z} E_z(k_z,\omega), \qquad (2)$$

where k_z and ω denote the wavenumber and angular frequency, respectively. In practice, the scaling in the $f-k_z$ domain gives rise to numerical instabilities for k_z values approaching zero. This can be remediated by computing instead

$$V_z^{\rm DAS}(k_z,\omega) = -\frac{\omega + \Delta}{k_z + \Delta} E_z(k_z,\omega), \tag{3}$$

where Δ is a scalar parameter for stabilization. As proposed in Lindsey et al. (2020), Δ can be determined relatively to the peak ground velocity value as measured by a colocated conventional seismometer.

Estimation of the DAS system response in the frequency domain

We can define the observed DAS-derived velocity response in terms of the convolution between a reference response $V_{\rm ref}$ with the DAS system response H^{DAS} . This can be expressed at any depth along the fiber and in the frequency domain by

$$V_z^{\rm DAS}(z,\omega) = H^{\rm DAS}(z,\omega)V_z^{\rm ref}(z,\omega). \tag{4}$$

Only the vertical component is considered in equation 4. Here, V_z^{ref} can be estimated from a known and collocated instrument for which we have the observation and a known instrument response. This reference ground-velocity record can then be deconvolved from the DAS record to obtain an estimation of the DAS system response as follows:

$$H^{\rm DAS}(z,\omega) = \frac{V_z^{\rm DAS}(z,\omega)}{V_z^{\rm ref}(z,\omega)}.$$
 (5)

In practice, the domain of validity of H^{DAS} is limited to a frequency range for which the DAS and reference records contain sufficient seismic energy with respect to instrument noise levels.

The DAS system response removal

Once an estimation of the DAS system response is obtained from the application of equation 5, it can be used to deconvolve DAS velocity records obtained from the application of equation 3. This deconvolution can be formulated as follows:

$$V_z^{\mathrm{DAS,corr}}(z,\omega) = \frac{V_z^{\mathrm{DAS}}(z,\omega)}{H^{\mathrm{DAS}}(z,\omega)},$$
 (6)

where $V_z^{\text{DAS,corr}}$ denotes the corrected ground-velocity record obtained from DAS measurements initially expressed in strain units, as a result of the removal of the estimated response. The result can be directly interpreted in terms of ground velocity within the matching frequency range of the DAS and reference instrument(s).

RESULTS

The DAS-based velocity records

First, the DAS strain rate and acceleration data sets are transformed into strain and velocity records, respectively, via time integration. Then the f-kz rescaling procedure, as summarized in equation 3, is applied to groups of 151 adjacent DAS channels centered at each of the considered colocated depth positions. The stabilization scalar Δ is set equal to the peak velocity amplitude observed at the colocated sensor. Figure 3 shows the example of this rescaling for the DAS records of perforation shot 1 at position 8 (see position in Figure 2). In spite of preventing most of the numerical instabilities, the stabilization does not fully suppress the overboosted very-near-zero k_z components (Figure 3b). Because severe distortions would be introduced in the converted signals otherwise, these components are further attenuated using a cosine taper

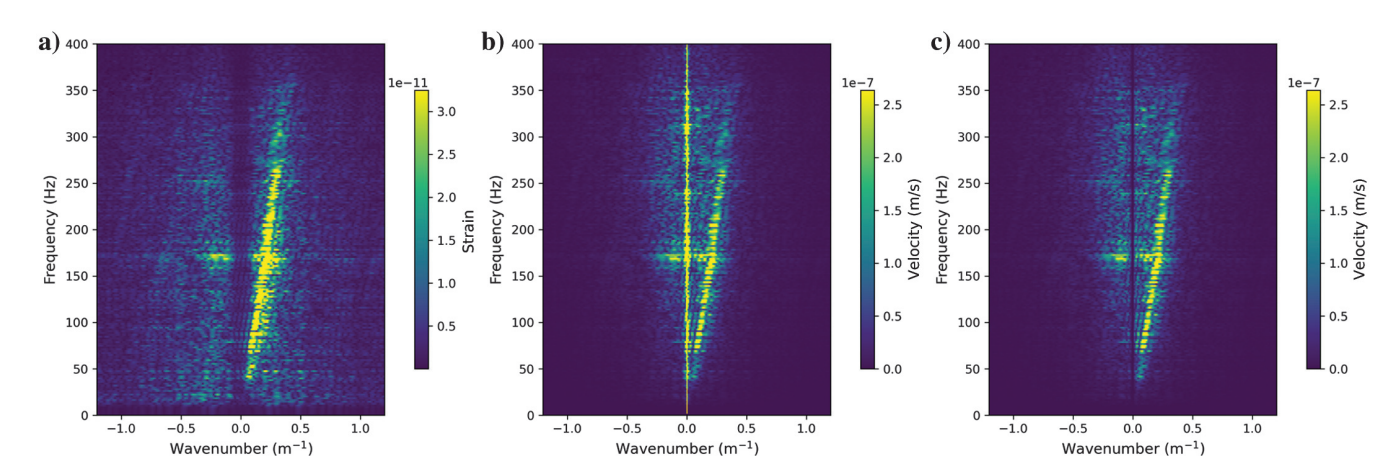


Figure 3. The DAS strain data rescaling in the f-k domain for perforation shot 1 and position 8, using 151 adjacent channels. (a) Amplitude spectrum in the f- k_z domain, (b) amplitude spectrum after rescaling with equation 3, and (c) after additional tapering for $k_z = 0$.

L79

(Figure 3c) before applying the Fourier transformations back to the time domain.

Time-domain results of the $f-k_z$ rescaling operations are shown in Figure 4 for the two perforation shots and the two DAS channels corresponding to the colocated depth positions 5 and 8. Overall, we observe a good match between the DAS-based velocity records and their corresponding reference velocity records, in terms of phase and amplitude. The strain records initially in the range from -0.05 to 0.05 nm/m are successfully rescaled to the reference velocity scale (-3e-7 to 3e-7 m/s) and the quality of the match is comparable for the two seismic events, highlighting the stability of repeated transformations.

This shows that the implemented $f-k_z$ rescaling operations retrieve relatively good estimates of ground motion records without introducing significant additional noise artifacts, provided that the strain records from the DAS channels are not initially overcontaminated with noise. As already shown in Figure 2, the latter condition is not fulfilled on certain DAS intervals and would therefore cause faulty retrievals of DAS-velocity records. In fact, poorer results are systematically obtained when noisy channel(s) are included in the selected group of adjacent channels. For this data set, the number of 151 DAS channels is found to preserve locally favorable noise conditions while sampling the wavenumber dimension with sufficient density for the $f-k_z$ transformation.

In spite of the matching velocity scale, discrepancies between the DAS and reference velocity records are clearly visible: in particular, the main peak amplitudes are substantially underestimated. In the following section, this remaining gap is quantified in terms of a DAS system response or transfer function, which can be further used to correct DAS velocity records and thus provide accurate particle-velocity records, as if obtained from the reference accelerometers.

The DAS system response

Figure 5 shows the estimated DAS response in the 20-200 Hz frequency range by applying equation 5 to the colocated velocity records of perforation shot 1 at depth position 8 (records in Figure 4a). The input signals as well as the derived response are quantified in terms of amplitude and phase spectra. In spite of few outlier values, we observe that the estimated response do not generally exceed the range of -20 to +5 dB for the amplitude response and of $-\pi/2$ and $+\pi/2$ radians for the phase response. The amplitude response (Figure 5c) remains mostly contained between −10 and 0 dB in the 80-200 Hz range while it clearly follows a downgoing trend toward -20 dB with decreasing frequencies. These apparent deviations from the 0 dB and 0 radians response (flat

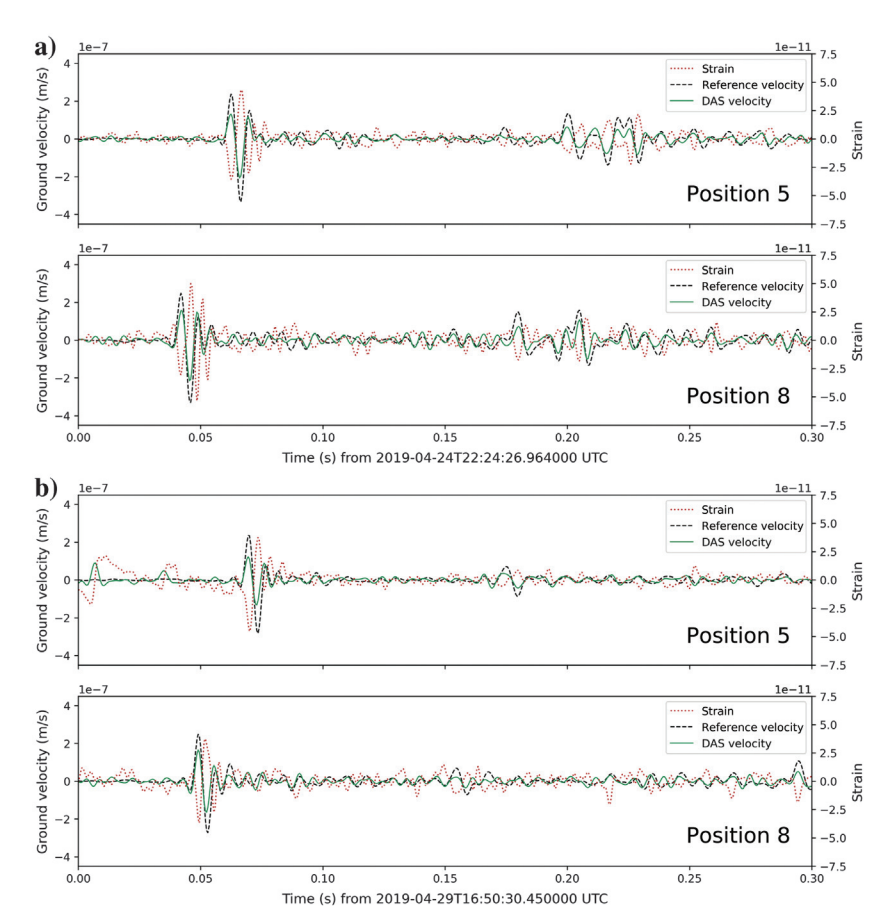


Figure 4. Conversion results of DAS strain records in velocity units for colocated positions 5 and 8 for (a) perforation shot 1 and (b) perforation shot 2, respectively.

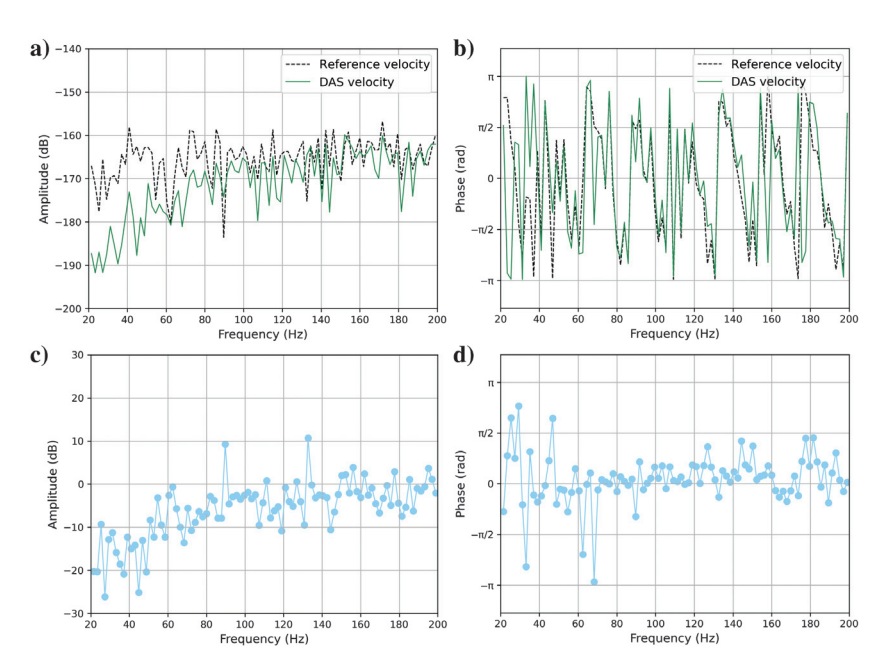


Figure 5. Retrieved individual DAS response using position 8 from perforation shot 1 (records in Figure 4a). (a and b) Amplitude and phase spectra of DAS (green) and geophone reference (black) velocity records and (c and d) estimated amplitude and phase response (blue) from application of equation 5.

response) are a frequency-domain representation, and so an explanation of the observed mismatches between the DAS and reference velocity records in Figure 4a.

To obtain a more stable and generalizable DAS system response, we average individual responses over several colocated positions over the two perforation shots. Figure 6 shows the selected responses for the two perforation shots and the resulting averages. Figure 6a and 6b shows amplitude and phase spectra for six depth positions (positions 1, 2, 5, 6, 7, and 8 in Figure 2) as well as those of the mean DAS response for perforation shot 1. The results from using perforation shot 2 are shown in Figure 6c and 6d. The general trend does not vary significantly across the selected positions, which shows a relative consistency between the individually estimated responses. We can interpret the differences as being mainly caused by the inevitable presence of noise, sometimes even coherent, in the input velocity records, which vary between the selected positions. But we also cannot exclude that part of these differences can be due as well to minor variations of the coupling conditions of the fiber and/or of the accelerometers across the depth range of interest.

As a result of averaging the individual responses, we obtain smoother DAS responses that account for the sensing conditions

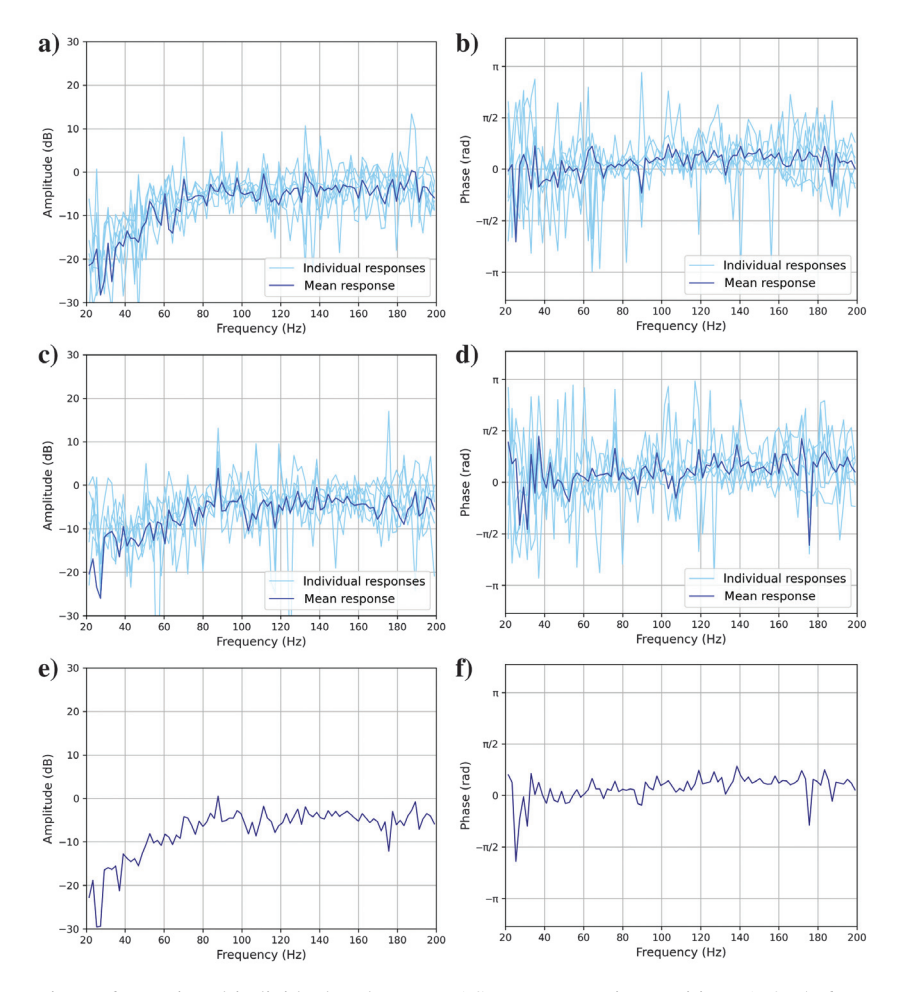


Figure 6. Retrieved individual and mean DAS responses using positions 1, 2, 5, 6, 7, and 8. (a and b) Amplitude and phase spectra of the retrieved individual and mean responses from perforation shot 1, (c and d) same as in (a and b) but for responses from perforation shot 2 and (e and f) amplitude and phase spectra of the average DAS system response between those of perforation shots 1 and 2

across a larger depth range. The mean responses from the two perforation shots are highly consistent. Below 80 Hz, the amplitude response tends to -20 dB, whereas it remains relatively stable at approximately -5 dB otherwise. The phase response gently oscillates approximately 0 dB across the entire frequency range. Therefore, the results from the two events are combined into a single sitespecific DAS system response. This final estimate of the average DAS system response, which is used in the next section to further calibrate the DAS-velocity records, is shown in Figure 6e and 6f. As intended, the largest inconsistencies between the two events are effectively reduced and the generalizability of the response is expected to be improved.

Calibrated DAS ground-velocity records

Using the averaged DAS system response, DAS records converted to units of particle velocity can be further corrected (equation 6). We apply this calibration procedure to the DAS records of the 110 microseismic events. Note that these records are not used at all for the empirical estimation of the DAS system response. Figure 7 shows the deconvolution results in the 20-200 Hz bandwidth

for the selected $M_w = -0.68$ microseismic event and for DAS records at positions 5 and 8. The Pwave peak amplitudes of the initial DAS velocity initially underestimated by 30%-40% (at 0.08 and 0.05 s in top panels in Figure 7a and 7b) become considerably improved with a much more accurate match to the reference waveforms (bottom panels in Figure 7a and 7b). Although the noise level is slightly boosted in the process, the removal of the estimated DAS response leads overall to successful corrections of the DAS velocity records: important characteristics such as the peak velocity have become more reliable for interpretating the actual ground motion. In addition, despite the DAS system response being predominantly estimated based on the P-wave energy from the perforation shots, major amplitude improvements are also obtained for the S waves. This is particularly visible at the deeper position 8 (0.24 s in Figure 7b) where S waves are not yet severely attenuated.

Measuring moment magnitudes

For the 110 events identified by Lellouch et al. (2020), we estimate M_W in the frequency domain following the approach of Stork et al. (2014) and Butcher et al. (2020) for the accelerometer and DAS data sets. Recalculating M_W for the accelerometer data using the same method used to calculate DAS magnitudes allows DAS and accelerometer M_W to be directly compared. These events occur within a hypocentral distance range of 1270-1431 m from the monitoring borehole with magnitudes ranging between $M_W = -1.8$ and $M_W = -0.5$.

The DAS systems are sensitive to uniaxial strain along the fiber direction; therefore, understanding the polarization of the incoming waves is an important consideration when estimating magnitudes. As the events occur below the array, we would expect that the fiber will be most sensitive to incoming P waves. We validate this by considering the particle motion of the arrivals using the 3C accelerometers.

Using a 0.02 s window around the first arrival, we use a least-squares function to fit a straight line to the observed particle motion and calculate the incident angle for all 110 events. From this data set, we calculate the mean angle and standard deviation for each sensor (Figure 8). In general, we estimate consistent particle motion angles for all sensors, with the exception of sensor 9 (S9), which was observed to be faulty. Of the remaining sensors, all display a near-vertical incident angle apart from sensor 3 with an angle of 23°. Given this is a string of sensors, it appears unlikely that this will be an instrument orientation issue, and may instead reflect a local velocity anomaly, such as a low velocity zone. Due to these observed incidence angles, the DAS array has near maximum sensitivity to P-wave arrivals; therefore, we use these arrivals and not the S wave to measure M_W .

For both data sets we first convert the measurement units into displacement through integration, then manually identify P-wave arrivals. Records with no prominent P-wave arrivals must be discarded at this stage. After applying a 20% cosine edge taper, a 0.1 s window after the arrival is then transformed into the frequency domain using the multitapering techniques developed by Prieto et al. (2009) (Figure 9). In the frequency domain, the seismic moment (M_0) of a recorded seismic signal can be expressed (Havskov and Ottemoller, 2010) as

$$M_0 = \frac{4\pi\rho v^3 d\Omega_0}{R},\tag{7}$$

-1.0 -1.5

0.05

where d is the hypocentral distance, v is the velocity at the source, ρ is the rock density at the source (2.5 g/cm^3) , and R is the radiation pattern correction term. As we are using the P wave to measure M_W , an average radiation pattern correction of 0.44 is applied and v represents the P-wave velocity (5.7 km/s). The term Ω_0 is the low-level frequency level, and while this can be estimated using a Brune model (Brune, 1970), we find that the limited frequency range and non-uniform DAS frequency response introduce erroneous and unstable estimates. Instead, we estimate this parameter by measuring the maximum amplitude before the corner frequency of the spectra. This approach allows us to derive reliable estimates of M_W for events with relatively high S/N (event 103 in Figure 9). However, for events with $M_W < -1.1$, the DAS P-wave signals are not sufficiently strong compared with the noise levels (event 54 in Figure 9).

To ensure the reliability of this magnitude estimation approach in the presence of favorable S/N, we first calculate all the M_W values for the accelerometer array and compare it against catalogue values. In Figure 10a, we observed that there is a general consistency between the two data sets. Comparing the calculated DAS M_W against the ones from the accelerometer array (Figure 10b), there is a good agreement between the two data sets for events with $M_W > -1.0$ but we are only able to measure 38 events (with $M_W \ge -1.2$) due to the poorer S/N of the DAS. At lower magnitudes, the noise levels influence the measurement, and a general divergence between the different measurements is observed.

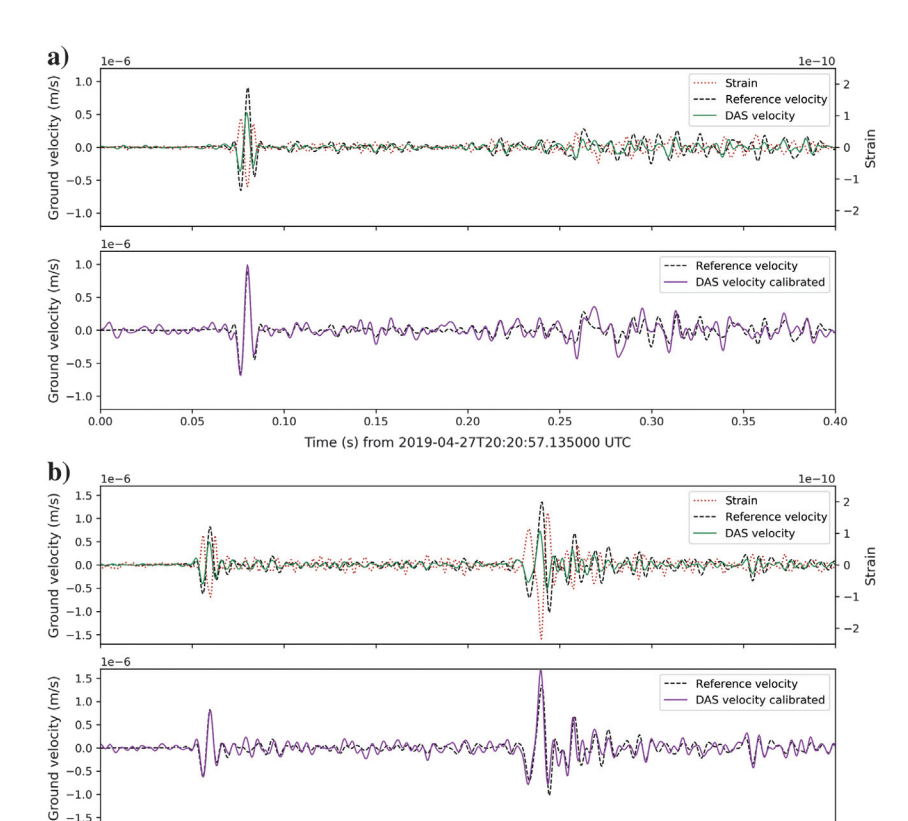
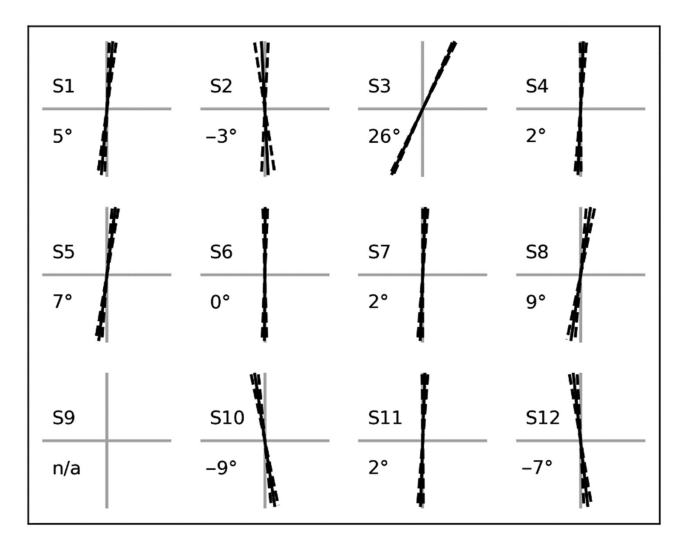


Figure 7. Calibration of DAS velocity records of the selected $M_w = -0.68$ microseismic event using the estimated mean DAS system response at (a) colocated position 5 and (b) colocated position 8.

0.20

Time (s) from 2019-04-27T20:20:57.135000 UTC

0.15



0.25

0.30

0.35

Figure 8. Mean particle motion (solid lines) and standard deviation (dashed lines) of 110 observed P-wave arrivals recorded on the accelerometers.

DISCUSSION

Using calibrated DAS records, we have been successfully able to determine M_W for microseismic events with $M_W > -1.0$, which are consistent with independently calculated M_W from accelerometer data. This demonstrates that once a site-specific DAS system response has been determined, DAS data can be independently used for moment magnitude calculation. For this, we perform a calibration by comparing particle-velocity records, which includes the time integration of the acceleration data produced by the reference instrumentation. Since the accelerometers have a flat response in acceleration in the 2-200 Hz range and the coupling quality is not perfectly known, we expect that the reference particle-velocity records are close but not exactly equal to the true ground velocity.

Previously, Lellouch et al. (2020) obtain local magnitude, M_L , estimations for the same set of microseismic events using the DAS

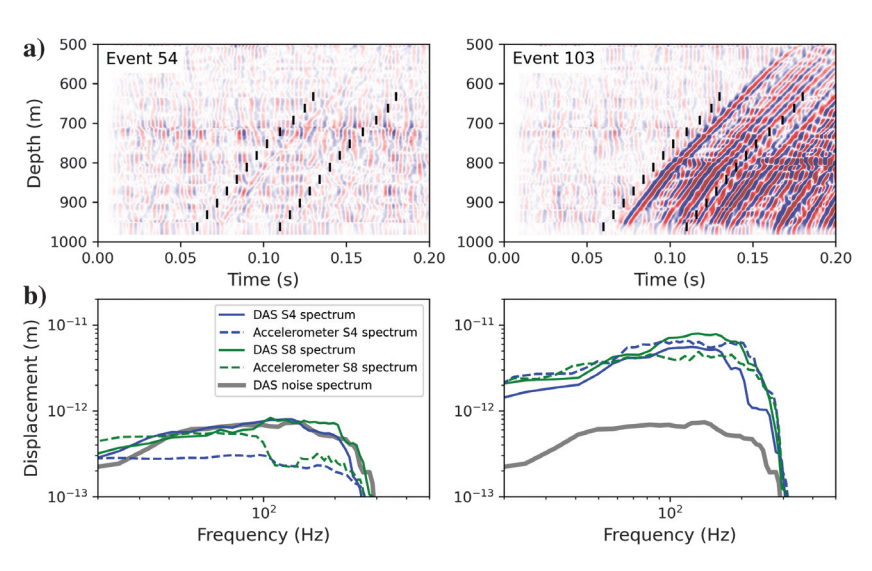


Figure 9. (a) Example of a $M_W = -1.2$ event (event 54) and $M_W = -0.6$ event (event 103) recorded on the DAS array. The P-wave windows used for magnitude estimation are indicated by local solid vertical black lines. (b) The spectra for the DAS and the accelerometer records of these events are plotted alongside the DAS noise level.

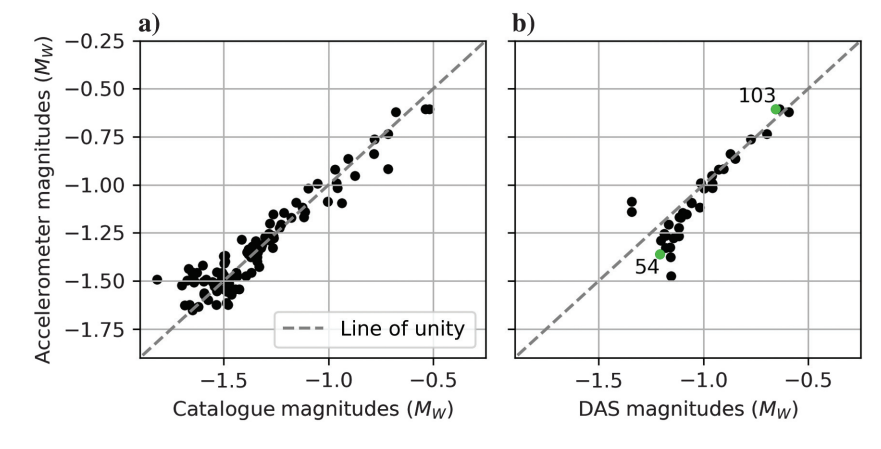


Figure 10. (a) Calculated magnitudes from the reference accelerometers plotted against the catalogued values (measurable for events with $M_W \ge -1.7$) and (b) DAS magnitudes plotted against the reference accelerometer data set for 38 events with $M_W \ge -1.2$. The green dots correspond to the two events explicitly shown in Figure 9.

data. Although comparing different magnitude scales, the results showed a strong linear correlation with the catalogue M_W from the accelerometers, with a correlation coefficient of 0.93. Their approach relies on an approximate empirical formula for local magnitude as a function of the largest recorded S-wave strain amplitude of the event. Distinctively, we use the P wave and determine M_W with a prior determination of the conversion of strain to ground motion units. One particular advantage of the moment magnitude estimation workflow is that it can better generalize to diverse locations and provides a magnitude estimate based on physical properties.

The conversion of strain measurements into velocity units by rescaling in the f- k_z domain does not allow direct retrieval of records accurately matching the reference particle-velocity records. The difference is subsequently interpreted in terms of a non-flat (0 dB and 0 radians) DAS system response, which includes coupling effects, cable effects, and other inner properties of the DAS system all to-

gether. However, we also expect that a minor part of the observed deviations from the flat response may be due to data-processing effects: during the preprocessing phase, the denoising of the DAS strain records in the f-k domain causes minor amplitude distortions of the signals; during the $f-k_z$ rescaling operation, the stabilization of equation 2 using the water-level parameter may also cause minor inaccuracies in the retrieved DAS velocity. Nevertheless, by verifying that the processing does not significantly distort the useful signals and is performed consistently for estimating the DAS system response and for calibrating microseismic events, these undesired effects do not hinder the retrieval of accurate DAS peak

A major part of the observed deviations can be linked to the difference of properties between the DAS and the reference instrumentation. In addition, the inner properties of the DAS optical system, differences that could cause at least part of these deviations are:

- · Orientation: although we assumed the downhole point-sensor string and the optical fiber to be perfectly vertically aligned in the well, this may not be exactly the case in practice, which would result in a difference of sensitivity between the optical fiber and the vertical component of the geophones for the same incoming seismic waves.
- · Angle sensitivity: for a P wave with incidence angle θ , the accelerometer vertical-component response is scaled by $cos(\theta)$, while the response of the DAS fiber is theoretically scaled by cos²(θ). However, this effect remains insignificant as the wavefields arrive at near-vertical incidence angles.
- Coupling: differences in formation coupling between the two devices can also explain part of the differences observed between the DAS velocity and reference records after applying the f-k rescaling operation. Moreover, imperfect ground coupling of the point-sensor device would cause

deviations of the corresponding reference records from the actual ground motion.

The computed individual DAS responses (Figure 6) do not vary considerably between the selected positions, which suggests only minor coupling differences for the fiber in the casing. The variation across the selected depth positions and across frequencies can be rather explained as the effect of the time and spatial variation of noise levels over DAS channels. To mitigate these local effects, we estimated an average response from two perforation shot events and six depth positions for each. This leads to a single depth-independent DAS system response, which proves to be reliable for correcting the DAS velocity records of the microseismic events. In that sense, incorporating records from more events could help refine the DAS system response by further removing event-specific effects.

However, the incorporation of further event recordings would provide better averaging to obtain stable, depth-dependent DAS system responses. Such a strategy is not explicitly tested in this study but can potentially result in locally calibrated records with even more accurate particle-velocity estimates. This would be especially required when the coupling conditions present substantial spatial variations along the fiber. The success of obtaining local DAS system responses generalizable to unseen events will rely on the use of a sufficient number of independent DAS records to mitigate the noisy conditions.

In general, the demonstrated DAS calibration workflow can be applied during the first phase of monitoring campaigns. This involves only the temporary deployment of reference seismic sensor(s) with known instrument response. Such DAS application is expected to be especially useful in harsh environments where traditional sensors would fail to meet the longevity required in long-term monitoring operations.

CONCLUSION

We have applied a workflow to empirically determine the transfer function of a DAS system based on a downhole, high-frequency seismic experiment. Using the calibrated signal, we then show that we can obtain reliable measurements of the moment magnitude from the DAS records down to $M_W = -1.0$. The workflow relies on the comparison between DAS measurements along the optical fiber and reference ground motion records from colocated point sensors. The prior step of converting strain measurements into velocity units is performed using a rescaling in the frequency-wavenumber domain. The colocated DAS-based velocity and reference groundvelocity records derived from accelerometer records are then used to calculate and analyze the DAS system response in the 20-200 Hz range, for which the response of the reference accelerometers is reliably known. In a second stage, we combined the estimates of individual DAS responses from two perforation shots over a depth range of more than 200 m to obtain a depth-independent DAS response and use it to calibrate ground-velocity records of microseismic events. Despite limited S/N in the input records, the calibration results show that the removal of the estimated site-specific DAS system response enables an improved match of the DAS-based velocity with the reference records. We expect that the estimation of the DAS system response can be refined by averaging over more seismic records and/or retain several local responses according to the positions with colocated reference records. This study, based on a downhole seismic sensing configuration, further demonstrates the possibilities to retrieve consistent ground motion records and moment magnitude estimates from DAS strain measurements using an empirical DAS transfer function workflow.

DATA AND MATERIALS AVAILABILITY

All the data used in this study are accessible via the Geothermal Data Repository from the U.S. Department of Energy (https://gdr .openei.org/). The microseismic event catalogue can be downloaded from https://gdr.openei.org/submissions/1151. Instructions on how to download the accelerometer and DAS data can be found at https:// gdr.openei.org/submissions/1207 and at https://gdr.openei.org/ submissions/1185, respectively

In particular, the following unix shell commands download .sgy files containing the raw DAS data shown in Figure 2 after preprocessing:

-q https://pando-rgw01.chpc.utah.edu/silixa_das_apr_24_ wget 2019/FORGE_78-32_iDASv3-P11_UTC190424222424.sgy

wget -q https://pando-rgw01.chpc.utah.edu/silixa_das_apr_29_ 2019/FORGE_78-32_iDASv3-P11_UTC190429165023.sgy

wget -q https://pando-rgw01.chpc.utah.edu/silixa_das_apr_27_ 2019/FORGE 78-32 iDASv3-P11 UTC190427202053.sgv

And the following commands will download .segy files containing the raw accelerometer data shown in Figure 2 after preprocessing:

wget -q https://pando-rgw01.chpc.utah.edu/slb_2019_MW78-32_010/20190424222422.196.segy

wget -q https://pando-rgw01.chpc.utah.edu/slb_2019_MW78-32_018/20190429165015.562.segy

wget -q https://pando-rgw01.chpc.utah.edu/slb_2019_MW78-32_014/20190427202045.868.segy.

ACKNOWLEDGMENTS

We thank A. Lellouch for providing guidance in the retrieval of relevant data from the FORGE field laboratory. This research was carried out as part of the project "Digital Monitoring of CO2 storage projects" (DigiMon, project no. 299622), which is part of the ERA-NET and Accelerating CCS Technologies (ACT2) program.

REFERENCES

Ajo-Franklin, J. B., S. Dou, N. J. Lindsey, I. Monga, C. Tracy, M. Robertson, V. R. Tribaldos, C. Ulrich, B. Freifeld, T. Daley, and X. Li, 2019, Distributed acoustic sensing using dark fiber for near-surface characterization and broadband seismic event detection: Scientific Reports, 9, 1328, doi:

Aki, K., and P. G. Richards, 2002, Quantitative seismology, 2nd ed.: University Science Books.

Bóna, A., T. Dean, J. Correa, R. Pevzner, K. V. Tertyshnikov, and L. Van Zaanen, 2017, Amplitude and phase response of DAS receivers: 79th Annual International Conference and Exhibition, EAGE, Extended Abstracts, doi: 10.3997/2214-4609.201701200.

Brune, J. N., 1970, Tectonic stress and the spectra of seismic shear waves from earthquakes: Journal of Geophysical Research, 75, 4997–5009, doi:

Butcher, A., R. Luckett, J.-M. Kendall, and B. Baptie, 2020, Seismic magnitudes, corner frequencies, and microseismicity: Using ambient noise to correct for high-frequency attenuation: Bulletin of the Seismological Society of America, **110**, 1260–1275, doi: 10.1785/0120190032.

Cole, S., M. Karrenbach, D. Kahn, J. Rich, K. Silver, and D. Langton, 2018, Source parameter estimation from DAS microseismic data: 88th Annual International Meeting, SEG, Expanded Abstracts, 4928-4932, doi: 10

Daley, T. M., D. E. Miller, K. Dodds, P. Cook, and B. M. Freifeld, 2016, Field testing of modular borehole monitoring with simultaneous

- distributed acoustic sensing and geophone vertical seismic profiles at Citronelle, Alabama: Geophysical Prospecting, 64, 1318–1334, doi: 10
- Daley, T. M., M. Robertson, B. M. Freifeld, D. White, D. E. Miller, F. Herkenhoff, and J. Cocker, 2014. Simultaneous acquisition of distributed acoustic sensing VSP with multi-mode and single-mode fiber optic cables and 3-component geophones at the Aquistore CO2 storage site: 84th Annual International Meeting, SEG, Expanded Abstracts, 5014–5018, doi: 10.1190/segam2014-1357.1
- Havskov, J., and L. Ottemoller, 2010, Routine data processing in earthquake seismology: Springer.
- Hudson, T. S., A. F. Baird, J. M. Kendall, S. K. Kufner, A. M. Brisbourne, A. M. Smith, A. Butcher, A. Chalari, and A. Clarke, 2021, Distributed Acoustic Sensing (DAS) for natural microseismicity studies: A case study from Antarctica: Journal of Geophysical Research: Solid Earth, 126, e2020JB021493,
- Jousset, P., T. Reinsch, T. Ryberg, H. Blanck, A. Clarke, R. Aghayev, G. P. Hersir, J. Henninges, M. Weber, and C. M. Krawczyk, 2018, Dynamic strain determination using fibre-optic cables allows imaging of seismological and structural features: Nature Communications, 9, 2509, doi: 10.1038/s41467-018-04860-y
- Karrenbach, M., S. Cole, A. Ridge, K. Boone, D. Kahn, J. Rich, K. Silver, and D. Langton, 2019, Fiber-optic distributed acoustic sensing of microseismicity, strain and temperature during hydraulic fracturing: Geophys-
- ics, **84**, no. 1, D11–D23, doi: 10.1190/geo2017-0396.1. Kendall, J.-M., A. Butcher, A. L. Stork, J. P. Verdon, R. Luckett, and B. J. Baptie, 2019, How big is a small earthquake? Challenges in determining microseismic magnitudes: First Break, 37, 51-56, doi: 10.3997/1365
- Lellouch, A., N. J. Lindsey, W. L. Ellsworth, and B. L. Biondi, 2020, Comparison between distributed acoustic sensing and geophones: Downhole microseismic monitoring of the FORGE geothermal experiment: Seismological Research Letters, **91**, 3256–3268, doi: 10.1785/0220200149. Lellouch, A., S. Yuan, W. L. Ellsworth, and B. Biondi, 2019, Velocity-based
- earthquake detection using downhole distributed acoustic sensing Examples from the San Andreas Fault Observatory at Depth: Bulletin of the Seismological Society of America, 109, 2491-2500, doi: 10.1785/
- Lindsey, N. J., E. Martin, D. Dreger, B. Freifeld, S. Cole, S. James, B. Biondi, and J. B. Ajo-Franklin, 2017, Fiber-optic network observations of earthquake wavefields: Geophysical Research Letters, 44, 11792-11799, doi: 10.1002/2017GL07
- Lindsey, N. J., H. Rademacher, and J. B. Ajo-Franklin, 2020, On the broadband instrument response of fiber-optic DAS arrays: Journal of Geophysical Research: Solid Earth, 125, e2019JB018145, doi: 10.1029/2019JB018145.
- Lior, I., D. Rivet, J. P. Ampuero, A. Sladen, S. Barrientos, R. Sánchez-Olavarría, G. A. Villarroel Opazo, and J. A. Bustamante Prado, 2023, Magnitude estimation and ground motion prediction to harness fiber optic distributed acoustic sensing for earthquake early warning: Scientific Reports, 13, 424, doi: 10.1038/s41598-023-27444-3.
- Martin, E. R., C. M. Castillo, S. Cole, P. S. Sawasdee, S. Yuan, R. Clapp, M. Karrenbach, and B. L. Biondi, 2017, Seismic monitoring leveraging existing telecom infrastructure at the SDASA: Active, passive, and

- ambient-noise analysis: The Leading Edge, 36, 1025-1031, doi: 10
- Mateeva, A., J. Lopez, J. Mestayer, P. Wills, B. Cox, D. Kiyashchenko, Z. Yang, W. Berlang, R. Detomo, and S. Grandi, 2013, Distributed acoustic sensing for reservoir monitoring with VSP: The Leading Edge, 32, 1278-1283, doi: 10.1190/tle32101278.1
- Mateeva, A., J. Lopez, H. Potters, J. Mestayer, B. Cox, D. Kiyashchenko, P. Wills, S. Grandi, K. Hornman, B. Kuvshinov, W. Berlang, Z. Yang, and R. Detomo, 2014, Distributed acoustic sensing for reservoir monitoring with vertical seismic profiling: Geophysical Prospecting, 62, 679–692, doi: 10 8.12116
- Miller, D., T. Coleman, X. Zeng, J. Patterson, E. Reinisch, H. Wang, D. Fratta, W. Trainor-Guitton, C. Thurber, M. Robertson, K. Feigl, and The PoroTomo Team, 2018, DAS and DTS at Brady Hot Springs: Observations about coupling and coupled interpretations: 43rd Stanford Workshop
- on Geothermal Reservoir Engineering.

 Moore, J., S. Simmons, J. McLennan, C. Jones, G. Skowron, P. Wannnamaker, G. Nash, C. Hardwick, W. Hurlbut, R. Allis, and S. Kirby, 2019, Utah FORGE phase 2C topical report: Energy and Geoscience Institute at the University of Utah.
- Nayak, A., J. Correa, and J. Ajo-Franklin, 2024, Seismic magnitude estimation using low-frequency strain amplitudes recorded by DAS arrays at farfield distances: Bulletin of the Seismological Society of America, 114, 1818–1838, doi: 10.1785/0120230318.
- Paitz, P., P. Edme, D. Gräff, F. Walter, J. Doetsch, A. Chalari, C. Schmelzbach, and A. Fichtner, 2021, Empirical investigations of the instrument response for distributed acoustic sensing (DAS) across 17 octaves: Bulletin of the Seismological Society of America, **111**, 1–10, doi: 10.1785/0120200185.
- Prieto, G. A., R. L. Parker, and F. L. Vernon, 2009, A Fortran 90 library for multitaper spectrum analysis: Computers and Geosciences, 35, 1701–1710, doi: 10.1016/j.cageo.2008.06.007.
- Stork, A. L., J. P. Verdon, and J.-M. Kendall, 2014, The robustness of seismic moment and magnitudes estimated using spectral analysis: Geophysical Prospecting, **62**, 862–878, doi: 10.1111/1365-2478.12134.
- Wang, H. F., X. Zeng, D. E. Miller, D. Fratta, K. L. Feigl, C. H. Thurber, and R. J. Mellors, 2018, Ground motion response to an ML 4.3 earthquake using co-located distributed acoustic sensing and seismometer arrays: Geophysical Journal International, **213**, 2020–2036, doi: 10.1093/gji/ggy102. Yin, J., W. Zhu, J. Li, E. Biondi, Y. Miao, Z. J. Spica, L. Viens, M. Shino-
- hara, S. Ide, K. Mochizuki, and A. L. Husker, 2023, Earthquake magnitude with DAS: A transferable data-based scaling relation: Geophysical Research Letters, **50**, e2023GL103045, doi: 10.1029/2023GL103045. Zhou, W., A. Butcher, A. M. Brisbourne, S.-K. Kufner, J.-M. Kendall, and
- A. L. Stork, 2022, Seismic noise interferometry and distributed acoustic sensing (DAS): Inverting for the firn layer S-velocity structure on Rutford Ice Stream, Antarctica: Journal of Geophysical Research: Earth Surface, 127, e2022JF006917, doi: 10.1029/2022JF006917.
- Zulic, S., E. Sidenko, A. Yurikov, K. Tertyshnikov, A. Bona, and R. Pevzner, 2022, Comparison of amplitude measurements on borehole geophone and DAS data: Sensors, 22, 9510, doi: 10.3390/s22239510.

Biographies and photographs of the authors are not available.